Influence of water vapor impurities and gas temperature on the 1.73 μm atomic xenon laser

H. Tomizawa,* M. Salvermoser,++ J. Wieser,+ and A. Ulrich+

** Research Laboratory for Nuclear Reactors, Tokyo Institute of Technology, 2–12–1 Ohokayama Meguro-ku, Tokyo 152–8550, Japan*

+ Technische Universit×d×t M×u×nchen, James-Franck Str. 1 D–85747 Garching, Germany

++ Department of Physics, Rutgers University, Newark, New Jersey 07102

Received June 30, 1999

High power Ar–Xe laser devices often face the problem of premature termination of laser output power with respect to the pumping pulse. Several reasons, including temperature effects, outgassing of impurities from walls as well as electron induced effects have been discussed. Here, two experiments, elucidating the influence of water vapor content in the lasing gas mixture on laser output power and laser threshold, and the effect of temperature rise in the laser gas on amplitude and shape of the laser output pulse, have been performed at the Munich Tandem accelerator, using 100 MeV $^{32}S^{9+}$ beams for pumping, thus simulating nuclear pumped laser (NPL) experiments at a pumping power density of ~100 W/cm^3. To study the influence of water vapor on laser parameters, highly purified 500 mbar Ar gas containing 0.5% Xe was used with well defined amounts of water vapor added. A continuous decrease of laser power was observed with increasing water concentration. A simple model is used to explain the data. Rate constants for quenching the upper level ($K^Q_{H_2O}$), and a ratio of the rate constant for electron attachment to water vapor to the total recombination rate of $4\cdot10^{-9}$ cm^3/s and $6\cdot10^{-16}$ cm^3, respectively, were obtained from this model. The second experiment has been performed, using ultra-high purity laser gases to measure the temperature dependence of laser output. The laser gas mixture, containing 327 mbar of Ar and 3 mbar Xe at room temperature, was pumped using rectangular 50 μs pulses (rise time ~100 ns) of 100 MeV $^{32}S^{9+}$ ions. In a pure Ar–Xe mixture, a decrease of laser output power with increasing temperature could be observed. Extreme afterglow lasing, reaching more than 20% of the entire energy in the 50 μs laser output and lasting for more than 20 μs was observed in the temperature range between 400 K and 570 K.

1. Introduction

Laser operation on the 1.73 μm transition in xenon atoms has been studied extensively.[1–6] Recently a very compact, low-energy electron beam pumped Ar–Xe laser[7] has been developed which may find application in atmospheric optics research, e.g., as a seeding laser in lidar systems. Up to now Ar–Xe lasers have mainly been studied as high power electron beam and so called nuclear pumped laser (NPL) systems.[8] This laser has a high efficiency (max. 8%)[9–11] and a low threshold.[12–13] It is a potentially high energy (up to about 100 kJ) NPL with pulse lengths of ~10 ms.[14] Despite the promising characteristics such as high efficiency a problem of atomic rare gas NPLs has become apparent since the early times of these lasers. Often, when high pumping power density was used, premature termination of the laser pulse was observed. Sometimes peak laser intensity was even reached prior to the peak of the pumping power pulse.[15–16] Recently, however the optical nuclear-pumped amplifier using the fast burst reactor (Bars–6) in Obninsk has shown significantly improved performance, most likely due to good gas purification.[17] The problem of limited reproducibility of the laser pulse[15–16,18] suggests that there are factors which strongly influence the performance of the laser but are not yet fully understood.

Several reasons for these problems have been discussed. Here, two main causes are considered for explaining these phenomena. Up to now most experiments and their analysis have dealt with the temperature dependence of the Ar–Xe laser. Electron collisional mixing (ECM)[19] has been suggested causing the temperature dependence. Modeling gas temperature dependence analytically is complicated and will not be described here. Some experiments concerning temperature dependence[20–22] have been performed during the last decade. However, there still seems to be lack of experimental data for performing accurate numerical modeling.

As an alternative to temperature dependence, A.A. Mavlyutov et al. discussed the influence of molecular water impurities in the laser gas mixture on the intensity of the atomic xenon laser and performed experiments on this issue.[23] The authors suggested that water molecules, desorbed from the walls of the laser cell, remove electrons by an electron attachment process, because water molecules are strongly electronegative. Therefore, the recombination rate is reduced. As a result, the gain of the laser decreases. In addition to the electron attachment process, we took collisional quenching of neutral excited xenon atoms by water molecules into consideration. Although the effect of electron attachment will turn out to be larger than that of collisional quenching of neutral excited xenon atoms by water molecules in reducing laser intensity, collisional quenching is not negligible in modeling the influence of water vapor impurities on laser output.

Experiments have been performed to study the influence of water vapor impurities in the laser gas mixture and gas temperature on the output power of the atomic xenon laser. During these experiments, all other parameters of the laser were kept fixed. The corresponding rate constants are derived using a rather a simple theoretical model for electron attachment with water vapor at room temperature.

0235-6880/00/03 213-07 $02.00

2. Experimental setup and concept

2.1. Experimental setup

Experiments were performed using a beam of 100 MeV $^{32}S^{9+}$ ions from the Munich Tandem van de Graff accelerator for pumping. The 20–50 μs long beam pulses were operated at repetition rates of 30–45 Hz. The laser gas mixture was separated from the beam line vacuum of the accelerator by a 1 mg/cm^2 titanium entrance foil with an aperture of 4-mm diameter (see Fig. 2). The pumping power density was on the order of 100 W/cm^3 which is comparable with the typical power density used in the NPL experiments. The beam pulses were formed using an electrostatic chopper installed at the low energy side of the accelerator. Using the signals from a digital pulsing and delay module for switching this chopper we could form rectangular pulses of the heavy ion beam with rise and fall times of less than 100 ns (see the pump pulse in Fig. 1). Laser output power reached its steady state value during the 20-μs pulse width.

A schematic drawing of the laser setup is shown in Fig. 2. The laser gas cell was built using standard stainless steel high vacuum components with 100-mm inner diameter. The titanium entrance foil allowed maintaining atmospheric pressure in the gas cell and at the same time a pressure of 10^{-6} mbar in the beam line. The absolute pressure of the laser gas mixture was measured using a capacitance manometer (Baratron, Type: 390HA–01000) with a sensor for a pressure region between 10^{-3} mbar and 1 bar. Using a sensitive electrical hygrometer (Panametrics, Model 708E), the water vapor densities were measured and controlled during experiments. The gas heater cell (G in Fig. 2) consisted of a 25-cm-long quartz cylinder with an inner diameter of 2 cm and a tungsten coil. It was installed in the gas cell to cover the region excited by the heavy ion beam. The gas temperatures inside (at the end and in the middle) and outside the gas heater cell were measured using the platinum resistance thermometers (T in Fig. 2). The laser gas was mixed using Ar and Xe with a minimum purity of 99.998%. The laser gases were mixtures of 0.5–1.0% xenon concentration with a total gas pressure of 300–500 mbar at room temperature.

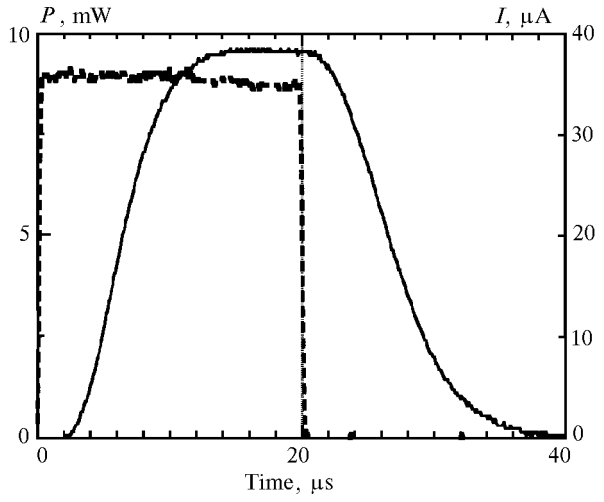

Fig. 1. Time dependence of laser output P (solid line) and pump pulse I (dotted line) for a pulse width of 20 μs. The beam current of about 36 μA corresponds to a pumping power of 400 W.

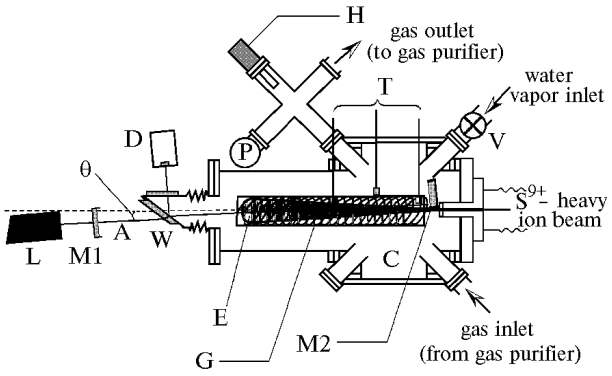

Fig. 2. Schematic drawing of the experimental setup: the beam line, laser optical axis (A), titanium entrance foil (F), excited region (E), gas cell (C), laser optics (L: alignment laser; M1, M2: mirror (rcc = 1.5, 10 m); W: Brewster window), pressure gauges (P), germanium photodiode detector (D), valve (V), hygrometer (H), platinum resistance thermometers (T), and gas heater cell (G) are shown. The angle (θ) between ion beam and laser axes was 1.2°.

A rare gas purifier operating with hot (800°C) titanium was installed between the gas outlet and inlet of the laser cell and purified laser gas mixtures were circulated through the system using a metal bellows compressor. Purification of the laser gas mixture is essential, especially as a prerequisite for measuring the influence of gas temperature alone.

Our purification system could realize a low water vapor density of $5\cdot10^{13}$ cm^{-3} even at 663 K, the maximum temperature of the gas mixture inside the gas heater cell. Water vapor effect on the laser output power is negligible at the water vapor number density of $5\cdot10^{13}$ cm^{-3}. The laser setup, schematically shown in Fig. 2, was similar to that used in previous experiments conducted at the Munich Tandem Accelerator.[24] The optical axis of the laser was tilted with respect to the ion beam axis at an angle for which laser output power reached is maximum. The unstable optical cavity consisted of narrow-band mirrors with the radius of curvature of 1.5 m and 10 m, respectively. Laser power was measured by measuring the output power transmitted through the external mirror and alternatively via reflections off from the Brewster window (W, Fig. 2). The germanium photodiode detector used was tested for linear response up to the laser output power of 10 mW. A correction factor was determined in an off-line experiment for converting the detector readouts into the laser output power for values above 10 mW.

2.2. Experimental concept and procedure

During the experiments, all parameters of the laser were kept constant except for one parameter which was varied deliberately (water vapor concentration or gas temperature). The first experiment was aimed at measuring the influence of water vapor impurities on the laser output. It is important for measuring the influence of water vapor alone, to maintain an almost constant gas temperature. Pumping the laser with 50-μs duration heavy ion beam pulses, the temperature of the laser gas mixture raised only by 10°C. On the other hand, it is important for measuring the influence of gas temperature alone that the lasing gas mixture is kept water-vapor-free and at a constant density. Using the equation of state for an ideal gas, the gas pressures, which correspond to constant density were calculated using the gas temperatures and were adjusted accordingly during each measurement.

2.2.1. Measurement of water vapor dependence of laser output

In the beginning of the experiment, laser operation was optimized and then water vapor was added to the laser gas by diffusion. For that purpose a valve (see Fig. 2) was opened to a section of the cell which had been partly filled with distilled water, pumped strongly until the water had frozen and a low pressure (~mbar) was reached. Then the section was brought back to room temperature. By this procedure it was assured that only water vapor was added to the laser gas. After adding the water vapor the laser had stopped operating. Using the gas purifier we then removed the water vapor from the laser gas step by step while measuring its concentration with the hygrometer and the corresponding laser output with a photodiode. The intensity of the heavy ion beam was kept constant. The measurements were performed whenever both the laser output power and hygrometer readings had stabilized.

In a separate experiment the laser parameters for a water-vapor-free laser gas mixture were determined by varying the cavity loss by varying the angle of incidence onto the Brewster window (W in Fig. 2). Additional cavity losses due to the reflection from the Brewster window surfaces were calculated using Fresnel's formula. The laser parameters as derived by this method were as follows: 18 W/cm^2 saturation intensity (I_s), 4.6% small-signal gain (g_0), and 1.3% cavity loss (*loss*) with the window at the end of the cell set to Brewster angle (quartz: 55.2° for 1.73 μm laser radiation) as it was done while measuring the influence of water vapor.

2.2.2. Measurement of the gas temperature dependence of laser output

In the beginning of the experiment the laser gas in the gas heater cell was heated up at the maximum temperature used in the experiment, controlling and actively purifying outgassing water vapor. The gas was kept at the maximum temperature, until the gas purifier had removed the water vapor from the laser gas. Water vapor concentration was measured using a hygrometer. When the gas mixture contained less than $1\cdot10^{13}$ cm^{-3} of water vapor density, the current through the heating coil was gradually reduced while measuring gas temperature with a platinum resistance thermometer and the corresponding laser output with a photodiode. The gas density was kept constant to avoid changing of the optical geometry and gas kinetics. Using the metal bellows compressor and the valves in the gas circulation system to control the total pressure of gas mixture in the gas cell, gas density was kept constant over the entire temperature region studied. Measurements were performed whenever both the laser output power and thermometer readouts had stabilized. By this procedure, at constant gas density, it was assured that only gas temperature affected the laser output. Finally, the cell was brought back to room temperature.

In a separate experiment the influence of the induced magnetic field from the solenoid coil of the gas heater cell (G in Figure 2) was checked using an external copper coil winding around the cell. No influence of the magnetic field on laser performance was observed over the entire experimental gas temperature region.

3. Experimental results

3.1. Dependence of the laser output on water vapor content

The influence of water vapor on the Ar–Xe laser was measured using 500 mbar total pressure and a xenon concentration of 0.5%. Relative laser intensity vs. water vapor contents in the laser gas mixture is shown in Fig. 3. The water vapor content of 0.01% corresponds to water vapor number concentration of the order of 10^{15} cm^{-3}. From this result it can be seen that the laser output is reduced as water vapor content increases. A significant effect is observed at the concentration higher than 10^{14} cm^{-3}. We observed a laser threshold at a water vapor density of about $3\cdot10^{15}$ cm^{-3}.

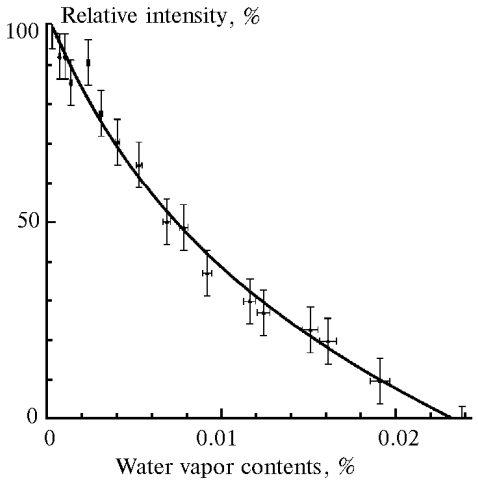

Fig. 3. Experimental result showing the influence of water vapor impurities on laser output: the relative laser intensity is plotted vs. water vapor contents. A fit to the data using a model as described in the text is also shown. According to this model, for example at the laser threshold, the electron attachment rate is 60% of the total electron depopulation rate and 30% of the total transition rate from the upper lasing level is due to quenching by water vapor which demonstrates that both processes play an important role.

3.2. Gas temperature dependence of the laser output

The experimental setup described here was designed for minimum optical cavity loss to perform experiments over a wide range of gas temperature (303~663 K) without reaching the laser threshold. The gas temperature dependence of the laser output power using Ar–Xe (0.9% Xe-concentration) gas mixture of $4.3\cdot10^{18}$ cm^{-3} constant density pumped by 30 and 50-μs pulse is shown in Fig. 4. Data shown here combine the results obtained using 30 and 50-μs duration pulses for pumping, respectively. Gas temperature here means the temperature in the middle of the gas heater cell. For a pure Ar–Xe mixture a decrease in the laser output power with the increasing temperature could be observed (see Fig. 4). In particular, the data show a significant reduction of the laser output power in the region of gas temperatures between 300 K and 400 K.

When using a gas mixture of higher density, we observed that the shape of the output laser pulse changed with gas

temperature change. Extreme afterglow lasing, reaching more than 20% of the total energy in the 50-μs laser output and lasting for more than 20 μs could be observed in the temperature range between 400 K and 570 K. Laser output power and corresponding pumping pulse are shown in Fig. 5. It shows an extreme afterglow lasing at a gas temperature of 454 K and a gas density of $5.5 \cdot 10^{18}$ cm^{-3}. When the pumping pulse terminated, laser output even increased.

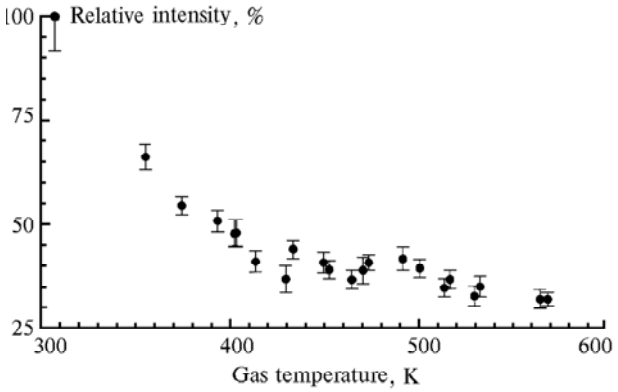

Fig. 4. Experimental results on the influence of gas temperature on the laser output: intensity of laser output is plotted vs. temperature of the laser gas. The laser gas was a mixture of 99.1% Ar and 0.9% Xe with $4.3 \cdot 10^{18}$ cm^{-3} constant density. All other parameters such as water vapor density (purity of lasing gas), optical geometry, xenon concentration, pumping power density were kept fixed.

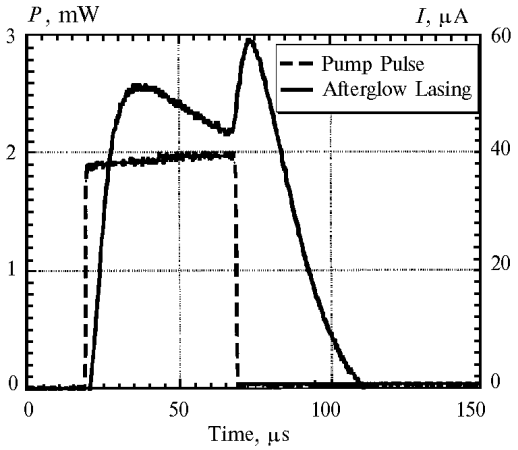

Fig. 5. Laser pulse observed in the gas temperature region between 400 and 570 K: time dependence of laser output power P (solid line) at a gas temperature of 454 K and a gas density of $5.5 \cdot 10^{18}$ cm^{-3}, and pump pulse intensity I (dotted line) for a pulse width of 50 μs are shown. The beam current of about 40 μA corresponds to a pumping power of 440 W.

4. Modeling the experimental data on the influence of water vapor impurities

Modeling of the complex temperature dependence has not been performed, yet. However, a rather simple model considering two mechanisms can describe the water vapor dependence of the Ar–Xe laser output very well. Saturation intensity (I_s) of the laser emission is given by

$$I_s = h\nu/\tau_l \sigma, \tag{1}$$

where h is the Planck's constant, ν is the frequency of laser radiation, τ is the lifetime of the upper lasing level, and σ is the stimulated emission cross section. The lifetime of the upper lasing level τ_l is given by

$$\tau_l^{-1} = A_{ik} + R^Q_{\text{upper}}, \tag{2}$$

where A_{ik} (as a short notation for $\sum_k A_{\text{upper}.\,k}$) are the spontaneous emission coefficients, and R^Q_{upper} the total quenching rate of the upper lasing level. The coefficients A_{ik} and the quenching rate coefficients of different energy levels of xenon were reported by Ohwa et al.[25] The radiative lifetime of the upper lasing level is $3 \cdot 10^5$ s^{-1}. The combined rates for collisional deexcitation, induced by thermalizing collisions within the 5d manifold with argon and xenon atoms, as discussed in the literature,[25] add up to $3.3 \cdot 10^7$ s^{-1} in the laser gas mixture used here (500 mbar, 0.5% Xe-concentration). The three body collision rates, as well as electron induced deexcitation rates can be neglected under the experimental conditions described here. The experimental data shown in Fig. 3 can be explained by two different processes: electron attachment and quenching of the upper lasing level by water vapor. A simplified pumping scheme of the Ar–Xe laser is shown in Fig. 3. The two processes considered as the main causes of a decrease in the laser output power are indicated.

Firstly, assuming that quenching of the upper lasing level by water molecules is the only cause for a reduction of the population of the upper lasing level, it has to be considered that small-signal gain g_0 and saturation intensity I_s are functions of water vapor densities [H_2O]. Since the population of the upper level, n_{upper} exceeds that of the lower one by more than one order of magnitude, the water vapor density dependences of g_0 and I_s are given by

$$g_0 = \sigma n_{\text{upper}} l = \frac{\sigma R_{\text{pump}}\, l}{A_{ik} + R^Q_{\text{upper}} + K^Q_{\text{H}_2\text{O}}[\text{H}_2\text{O}]}, \tag{3}$$

$$I_s = \frac{h\nu}{\sigma}\left(A_{ik} + R^Q_{\text{upper}} + K^Q_{\text{H}_2\text{O}}[\text{H}_2\text{O}]\right), \tag{4}$$

respectively, where R_{pump} is the pumping rate to the $5d[3/2]_1$, upper lasing level, R^Q_{upper} is the total quenching rate of the upper lasing level and σ is the cross section for stimulated emission. The rate constant $K^Q_{\text{H}_2\text{O}}$ is the quenching rate coefficient of water vapor. The parameter l is the net overlapping length of the optical mode volume with the active laser medium. The radiation intensity, I, inside the resonator is described using the laser parameters by the following formula:

$$I = \left(\frac{g_0}{loss} - 1\right) I_s. \tag{5}$$

By substituting Eqs. (3) and (4) into Eq. (5) the following dependence of I on [H_2O] is obtained:

$$I([\text{H}_2\text{O}]) = h\nu\left(\frac{R_{\text{pump}}\, l}{loss} - \frac{A_{ik} + R^Q_{\text{upper}} + K^Q_{\text{H}_2\text{O}}[\text{H}_2\text{O}]}{\text{s}}\right). \tag{6}$$

This linear dependence (6) of I on [H_2O] is equivalent to the reduction of the laser power upon addition of nitrogen described in the literature.[26] Note, that at this point it was

implicitly assumed that the water added to the laser gas can be treated as an ideal gas.

Data shown in Fig. 3, however, cannot be described by this linear dependence of I on $[H_2O]$. This indicates that quenching of the upper lasing level by water vapor is not the only relevant process and the electron attachment to water vapor must be considered.

Secondly, assuming that electron attachment is the only cause for a reduction of the population of the upper lasing level, only the small-signal gain g_0 is a function of water vapor densities $[H_2O]$ because only the pumping rate R_{pump} is influenced by water vapor (see Fig. 6).

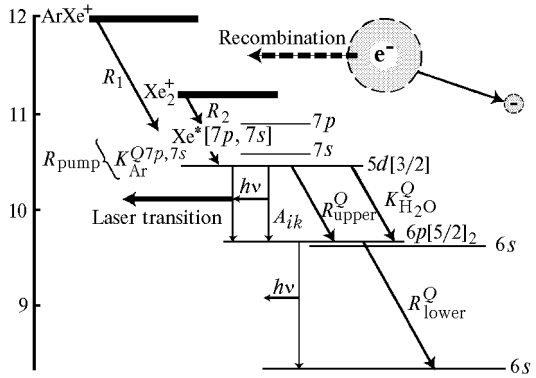

Fig. 6. Schematic level diagram: the excited xenon atoms (Xe*[7*p*,7s]), which are precursors of the upper lasing levels, molecular ion ($ArXe^+$, Xe_2^+) levels and the laser upper $5d[3/2]_1$, and lower $6p[5/2]_2$ levels are shown. Also, the dominant kinetic processes of the laser scheme considered here such as collisional quenching (constants: $K_{Ar}^{Q7p,7s}$, $K_{H_2O}^{Q}$; the total quenching rates of the upper and lower lasing level: R_{upper}^{Q}, R_{lower}^{Q}), dissociative recombinations (R_1, R_2), electron attachment to water vapor ($K_{H_2O}^{R}$), and optical transitions are shown. The rate R_{pump} is the pumping rate from the excited atomic xenon 7*p*- and 7*s*-levels to the upper lasing level.

The parameters g_0 and R_{pump} are proportional to the density of precursors of the upper lasing levels $[Xe^*_{7p,7s}]$:

$$g_0 \propto R_{pump} \propto [Xe^*_{7p,7s}] \quad . \tag{7}$$

The electrons in the laser plasma are produced by ionizing collisions of the heavy ion beam projectiles and secondary electrons with the target gas atoms, and are removed from the active volume by recombination with dimer ions Xe_2^+, $ArXe^+$, Ar_2^+, etc. Therefore, the electron density n_e is given by

$$n_e = \frac{R_{ionization}[Ar]}{K_{H_2O}^{R}[H_2O] + R(T_e)}, \tag{8}$$

where $R(T_e)$ is the sum over all recombination rates in this laser plasma which are functions of electron temperature T_e. The constant $K_{H_2O}^{R}$ is the electron attachment rate constant of water vapor. The rate $R_{ionization}$ is the sum over all types of ionization rates in the plasma. Excited xenon atoms at the 7*p*- and 7*s*-levels are formed via dissociative recombination with dimer ions Xe_2^+, $ArXe^+$. Then the excited xenon atoms in the 7*p*- and 7*s*-levels decay predominantly via collisional quenching with argon atoms. The production process of the dimer ions Xe_2^+, $ArXe^+$ is the preceding reaction for dissociative recombination. Note, that the densities of dimer ions $[Xe_2^+]$, $[ArXe^+]$ depend neither on the reduction of the electron densities n_e nor on the addition of water vapor, since the dimer ions decay predominantly to Xe_n^+ via collisions with argon and xenon atoms, and not via dissociative recombinations. The ratio between $[Xe^*_{7p,7s}]$ and n_e is described by the following formula:

$$[Xe^*_{7p,7s}] \cong \frac{F_{7p,7s}^{ArXe^+} K_{ArXe^+}^{R}[ArXe^+] + F_{7p,7s}^{Xe_2^+} K_{Xe_2^+}^{R}[Xe_2^+]}{K_{Ar}^{Q7p,7s}[Ar]} n_e \propto n_e, \tag{9}$$

where $F_{7p,7s}^{ArXe^+}$, $F_{7p,7s}^{Xe_2^+}$ are the constant fractions[12] of the reaction flux (R_1, R_2 in Figure 6) reaching the 7*p*- and 7*s*-levels from the dimer ions Xe_2^+, $ArXe^+$, respectively. The quantities $K_{ArXe^+}^{R}$, $K_{Xe_2^+}^{R}$ are the rate constants of the recombination of $ArXe^+$ and Xe_2^+, respectively, which are functions of electron and gas temperature. The quantity $K_{Ar}^{Q7p,7s}$ is the rate constant of quenching of the 7*p* and 7*s* excited levels of xenon by collisions with argon atoms.

Rearranging Eq. (7) by substituting Eq. (8) into Eq. (9), the dependence of g_0 on the water vapor density is given by

$$g_0 \propto R_{pump} = \frac{C_1}{K_{H_2O}^{R}[H_2O] + R(T_e)}, \tag{10}$$

where C_1 is a constant.

Fitting of formula (10) to the data reproduces the data shown in Fig. 3 in the region of small water vapor densities, but does not successfully describe the region near the laser threshold. Consequently both processes discussed above must be taken into account.

By substituting Eq. (10) into Eq. (6) a function $I([H_2O])$ is obtained

$$I([H_2O]) = \frac{h\nu}{\sigma}\left[\frac{C_2}{(K_{H_2O}^{R}/R(T_e))[H_2O]+1} - (A_{ik} + R_{upper}^{Q} + K_{H_2O}^{Q}[H_2O])\right], \tag{11}$$

where C_2 is the constant. The water vapor dependence (11) is used as a fitting function with the fitting parameters of C_2, $K_{H_2O}^{R}/R(T_e)$, and $K_{H_2O}^{Q}$ for our experimental data. The fitting result is shown in Fig. 3.

From the fitting results (solid curve in Figure 3), we obtain the rate constant of quenching by water vapor $K_{H_2O}^{Q}$ to be $4 \cdot 10^{-9}$ cm^3/s, and the ratio between the rate of electron attachment to water and all the recombination rates $K_{H_2O}^{R}/R(T_e)$ to be $6 \cdot 10^{-16}$ cm^3[H_2O].

5. Conclusion and discussion

Experiments have been conducted to study the influence of water vapor impurities and gas temperature on laser output, using 1.73 μm atomic xenon laser transition with Ar–Xe gas mixtures. The experimental data show a reduction of laser output power with the increasing gas temperature, at a constant gas density, and with the increasing water vapor density, at room temperature, independently. The experimental data show a significant reduction of the laser output power at water vapor

densities of the order of 10^{15} cm^{-3} (contents of 0.02%), and for gas temperature between 300 K and 400 K. This shows that both of these effects must be considered as the main causes of a premature termination of high power emission in Ar–Xe lasers.

Using simple modeling of the experimental data, water vapor quenching and electron attachment to water vapor are suggested as the main causes of the reduction of the output laser power, when water vapor is added to the laser gas. The quenching rate constant of water vapor $K^Q_{H_2O}$ of $4 \cdot 10^{-9}$ cm^3/s was obtained. From this model, however, an absolute value for the rate constant of electron attachment to the water vapor could not be described. For obtaining this absolute value it will be necessary to perform a complete modeling of the laser gas kinetics by use of a more detailed knowledge about water vapor and its reactions in the process. The mechanisms of the influence of water vapor can be more complicated than the simple model treated in this paper. In particular, nucleation of water vapor molecules due to the interactions between water vapor and ions in the laser gas may have to be taken into consideration.

The mechanisms influencing the lasing process via gas temperature alone are very complicated. All recombination rates, production rates of molecular ions, and electron collisional mixing in the manifold may have to be taken into consideration. Here, the effect of gas temperature has been measured for a laser operated in a water-vapor-free gas mixture. Actually the realistic, high power and long-pulse laser systems are important for understanding the mechanisms of the influence of water vapor on the laser output at high temperatures.

Acknowledgments

This work was funded by Tandem Accelerator laboratory Munich, NATO grant 921215, INTAS grant 96/351 and DAAD (Deutscher Akademischer Austauschdienst). Experiments were performed during H. Tomizawa's exchange program funded by DAAD. The authors acknowledge help by Mrs. B. Russ in designing and building the experimental setup. We also acknowledge the helpful support of the staff of Tandem Accelerator Laboratory, Munich and Fakultät für Physik E12, Technische Universität München.

References

1. O. Andrade, M. Gallardo, and K. Bockasten, Appl. Phys. Lett. **11**, No. 99 (1967).
2. P.L. Chapovskii, V.N. Lisitsyn, and A.R. Sorokin, Opt. Commun. **26**, No. 33 (1976).
3. S.A. Kochubei, V.N. Lisitsyn, A.R. Sorokin, and P.L. Chapovskii, Sov. J. Quantum Electron. **7**, No. 1142 (1978).
4. G.E. Courville, P.J. Walsh, and J.H. Wasko, J. Appl. Phys. **35**, No. 2547 (1964).
5. S.A. Lawton, J.B. Richards, L.A. Newmann, L. Specht, and T.A. DeTemple, J. Appl. Phys. **50**, No. 3888 (1979).
6. D.E. Rothe and K.O. Tan, Appl. Phys. Lett. **30**, No. 152 (1977).
7. A. Ulrich, C. Niessl, J. Wieser, H. Tomizawa, D.E. Murnick, and M. Salvermoser, J. Appl. Phys. **86**, No. 3525 (1999).
8. O.V. Sereda, V.F. Tarasenko, A.V. Fedenev, S.I. Yakovlenko, Quantum Electron. **23**, No. 459 (1993).
9. W.J. Witteman, S.W.A. Gielkens, V.N. Tskhai, P.J. Peters, in: *Proc. of Int. Conf. on Atomic and Molecular Pulsed Lasers II,* Sept. 22–26, 1997, Tomsk, Russia; V.A. Tarasenko, G.V. Mayer, and G.G. Petrash eds., Proc. SPIE **3403**, 11 (1997).
10. A.V. Karelin and O.V. Simakova, Laser Phys. **8**, No. 567 (1998); Preprint No. 9, Institute of General Physics, Russian Academy of Sciences, Moscow (1998).
11. G.A. Hebner and G.N. Hays, J. Appl. Phys. **65**, No. 3760 (1993).
12. A.M. Voinov, L.E. Dovbysh, V.N. Krivonosov, S.P. Mel'nikov, A.T. Kazakevich, I.V. Podmoshenkii, and A.A. Sinyanskii, Sov. Phys. Dokl. **24**, No. 189 (1979).
13. A.V. Karelin, Quantum Electron. **28**, No. 602 (1998).
14. P.P. Dyachenko, in: *Proc. of the 12th Int. Conf. on Laser Interaction and Related Plasma Phenomena,* Apr. 24–28, 1995, Osaka, Japan, Editors: S. Nakai, G.H. Miley, Osaka, Japan, 1995, ISBN 1–56396–624–7. Vol. 2, p. 894.
15. G.A. Hebner and G.N. Hays, J. Appl. Phys. **74**, No. 3673 (1993).
16. W.J. Alford and G.N. Hays, J. Appl. Phys. **65**, No. 3760 (1989).
17. P.P. Dyachenko, (private communication).
18. V.N. Kononov, M.V. Bokhovko, A.P. Budnik, I.V. Dobrovolskaya, and O.E. Kononov, in: *Proc. of the Ninth Int. Conf. on Emerging Nuclear Energy Systems,* June 28–July 2, 1998, Tel-Aviv, Israel, Editors: Y. Ronen, L. Teppers, and E. Elias. Vol. 2, p. 881.
19. M. Ohwa and M.J. Kushner, J. Quantum Electronics **26**, No. 1639 (1990).
20. A.I. Konak, S.P. Melnikov, V.V. Porkhaev, and A.A. Sinyanskii, Laser and Particle Beams **11**, No. 663 (1993).
21. G.A. Hebner, J.W. Shon, and M.J. Kushner, Appl. Phys. Lett. **63**, No. 2872 (1993).
22. G.A. Hebner, IEEE J. Quantum Electronics **31**, No. 1626 (1995).
23. A.A. Mavlyutov, A.I. Mis'kevich, and B.S. Salamakha, in: *Proc. of the 2nd Int. Conf. on Physics of Nuclear-Induced Plasma and Problems of Nuclear-Pumped Lasers* (NPL–94), Sept. 26–30, 1994, Arzamas-16, Russia, Editors: A.M. Voinov, S.P. Mel'nikov, A.A. Sinyanskii, VNIIEF, Arzamas–16, 1995, ISBN 5–85165–065–9. Vol. 1, p. 318.
24. A. Ulrich, H. Bolin, P. Kienle, and G.J. Perlow, Appl. Phys. Lett. **42**, No. 782 (1983).
25. M. Ohwa, T.J. Moratz, and M.J. Kushner, J. Appl. Phys. **66**, No. 5131 (1989).
26. N.G. Adams and D. Smith, Int. J. Mass. Spectrom. Ion Phys. **21**, No. 349 (1976).